Detecting the Signatures of Uranus and Neptune

Stephen R. Kane

NASA Exoplanet Science Institute, Caltech, MS 100-22, 770 South Wilson Avenue, Pasadena, CA 91125, USA

Abstract

With more than 15 years since the the first radial velocity discovery of a planet orbiting a Sun-like star, the time baseline for radial velocity surveys is now extending out beyond the orbit of Jupiter analogs. The sensitivity to exoplanet orbital periods beyond that of Saturn orbital radii however is still beyond our reach such that very few clues regarding the prevalence of ice giants orbiting solar analogs are available to us. Here we simulate the radial velocity, transit, and photometric phase amplitude signatures of the solar system giant planets, in particular Uranus and Neptune, and assess their detectability. We scale these results for application to monitoring low-mass stars and compare the relative detection prospects with other potential methods, such as astrometry and imaging. These results quantitatively show how many of the existing techniques are suitable for the detection of ice giants beyond the snow line for late-type stars and the challenges that lie ahead for the detection true Uranus/Neptune analogues around solar-type stars.

Keywords: Extrasolar planets, Uranus, Neptune

1. Introduction

Ice giant planets, such as Uranus and Neptune, have been known to exist for several hundred years. On July 10, 2011 one complete Neptunian orbit will have occurred since it was discovered on September 23, 1846 from the calculations of Le Verrier and Adams. Over the past 15 years, the number of planets known outside of our solar system has grown to be more than 500. Yet our time baseline combined with the sensitivity of our measurements have not yet allowed us to probe into regions of parameter space where we might discover ice giants around solar analogs. Microlensing surveys are

producing insights into the frequency of giant planets beyond the "snow line" (Gould et al., 2010), but statistics regarding the orbital properties of ice giants remains unknown and formation scenarios are deprived of the kinds of data that now exist for Jupiter analogs in exoplanetary systems.

The internal structure of Uranus and Neptune are known to differ quite dramatically from that of Jupiter and Saturn (Fortney et al., 2011). Much work has been performed on the formation mechanisms for the giant planets, but contention still remains between the competing ideas of core accretion and disk instability scenarios (see Matsuo et al. (2007) and references therein). The required timescales and current orbital configuration of the solar system giant planets favour a core accretion model, but the formation of Uranus and Neptune are still poorly understood (Benvenuto et al., 2009). Without other examples of ice giants to draw upon, it is difficult to understand where our ice giants formed, timescales for their migration, and their overall contributions to the orbital stability of the present solar system orbits.

As we approach the heliocentric birthday of Neptune's discovery, it is appropriate to ask how close we are to discovering a twin to Uranus or Neptune elsewhere. With instrumentation improvements of radial velocity surveys and time baselines now stretching out beyond the orbit of Jupiter, we are slowly entering a phase where the detection of Uranus and Neptune analogs is becoming more likely. Here we provide detailed detection simulations of our giant planets from an external perspective, concentrating on the detectability of Uranus and Neptune. We describe the expected radial velocity and photometric signatures and provide scaling laws for application to detection thresholds for ice giants orbiting late-type stars which serve as far more feasible targets in the short-term. We compare these to imaging and astrometric experiments and assess the relative detection prospects.

2. Formation of Ice Giants

The formation of Uranus and Neptune in situ is problematic using core accretion models due to the lack of disk material. A proposed solution builds the ice giants in the same vicinity as Jupiter whereupon they are scattered outwards once Jupiter develops its gas envelope (Thommes et al., 1999, 2002). Subsequent interactions with the Kuiper Belt is likely to have both stabilized and circularized the orbits of Uranus and Neptune to their present orbital configuration (Ford & Chiang, 2007; Levison et al., 2008). More detailed models of the formation mechanisms have since had success in ex-

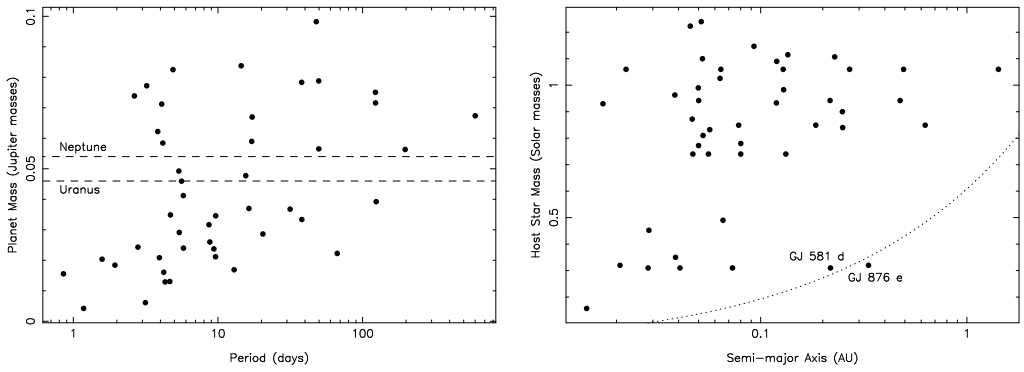

Figure 1: Known radial velocity planets with masses less than 0.1 Jupiter masses. Left: planet masses as a function of orbital period with Neptune and Uranus indicated by dashed lines. Right: Host star mass as a function of semi-major axis where the predicted snow-line is shown as a dotted line.

plaining the relative chemical abundances now seen in Uranus and Neptune (Dodson-Robinson et al., 2010).

Even though theories regarding the formation of Uranus and Neptune are becoming more sophisticated, these still remain the only ice giants for which we have detailed orbital information from which such models may be constructed. A key factor is the location of the "snow line", which is the radial distance from the center of a protostellar disk beyond which water molecules can efficiently condense to form ice. For our own system, this is approximately at the radius of the asteroid belt, $a \sim 2.7$ AU. The formation mechanisms required for the production of ice giants are therefore likely to be highly dependent upon the disk mass and the production of Jupiter analogs which may either disrupt their formation or scatter them to a larger semi-major axis. In exoplanetary systems, we can expect to find ice giants in a range of orbital configurations, including high eccentricities, depending upon their formation circumstances.

Ida & Lin (2005) approximate the location of the snow line as a function of stellar mass, $M_\star$, by $a_{\rm ice} = 2.7(M_\star/M_\odot)^2$. Kennedy et al. (2006) further develop the time-dependence of the snow line location in the context of low-mass stars. This work is extended by Kennedy & Kenyon (2008), in which the location of the snow line is generalized to stars of various masses. Using these models, one can investigate whether true ice giants, both in terms

of formation and composition, have already been detected around low-mass stars. Shown in Figure 1 are the known radial velocity exoplanets with masses in the vicinity of Uranus and Neptune. These data were extracted using the Exoplanet Data Explorer[1] and are current as of 1st January 2011. The left panel shows the minimum planet masses ($M_p \sin i$, where i is the orbital inclination) as a function of the orbital period, where the dashed lines indicate the masses of Uranus and Neptune for comparison. There have been a number of planets discovered with masses lower than the ice giants of our solar system, but these are preferentially found closer to their parent stars since this produces a larger radial velocity signature. The right panel shows the masses of the host stars for these planets as a function of the semi-major axis of the planetary orbits. The dotted line indicates the location of the snow line using the approximation of Ida & Lin (2005). The planet located just inside the snow line is GJ 581 d, a planet substantially less massive than Neptune ($\sim$ 7 Earth masses) and whose eccentric orbit takes it either side of the snow line as it passes between apastron and periastron (Mayor et al., 2009). A more analogous ice giant example is the case of GJ 876 e, shown just outside of the snow line. This planet has a mass between that of Uranus and Neptune and an almost circular orbit (Rivera et al., 2010). The existence of several more massive gas giants within the system at smaller orbital radii may indicate that migration during and after the formation of the ice giant also took place within this system (Boss, 2006, 2010).

3. Radial Velocity Signatures

3.1. The Signatures of Uranus and Neptune

The simulated data assume a precision of 10 cm/s with a cadence of one measurement per year over a complete Neptune orbit. We assume a cadence of one measurement per year over a complete Neptune orbit (164.8 years). The long-term stability of precision radial velocity instruments presents a significant challenge to achieving this. Recent examples include 10 years of observations of HD 185144 that were carried out using Keck/HIRES by Wright et al. (2008) from which they achieved an RMS scatter of the radial velocity variations of less than 2.5 m/s over the entire period. The HARPS instrument has already demonstrated stability of 1–2 m/s over the

[1] `http://exoplanets.org/`

timescale of months with further improvements expected in the near future (Pepe & Lovis, 2008). A long-term solution is the use of laser frequency combs (Li et al., 2008; Murphy et al., 2007) which can achieve long-term stability by stabilizing the frequency modes with the absolute frequencies of atomic clocks (Steinmetz et al., 2008; Udem et al., 2002).

Studies of intrinsic stellar variability and solar data show that many inactive stars exist, at least to the precision at which they have been studied (Wright, 2005), and that many types of activity may be circumvented (Boisse et al., 2011; Lagrange et al., 2010; Meunier et al., 2010). For example, star spot activity produces both radial velocity and photometric jitter. Star spots tend to persist for no longer than a few weeks for main sequence stars (Strassmeier, 2009) but their frequency rises and falls over longer timescales. The Sun has cycles of duration 11, 22, and 87 years for the Schwabe, Hale, and Gleissberg cycles respectively. These cycles can be identified and removed through simultaneous photometric and radial velocity monitoring and also through activity indicators for the star (Makarov et al., 2009). The star spot activity can also be tied to the stellar rotation periods which has been performed for numerous known exoplanet host stars (Simpson et al., 2010).

Figure 2 shows the result of the simulation for the solar system giant planets, first with all four planets and then systematically removing the signature of each planet in order of increasing orbital period until the combined signal of Uranus and Neptune remain. Data for the solar system planets were extracted from the JPL HORIZONS System[2]. The semi-amplitude of the radial velocity signal, K, is given by

$$K = \left(\frac{2\pi G}{P}\right)^{1/3} \frac{M_p \sin i}{(M_p + M_\star)^{2/3}} \frac{1}{\sqrt{1-e^2}} \tag{1}$$

where P is the period, i is the inclination of the planetary orbit, e is the orbital eccentricity, and M_p is the planetary mass. The inclination of the orbital plane to the observer line-of-sight is assumed to be edge-on ($i = 90°$). The semi-amplitude for each of the planets under these conditions is shown in Table 1.

In each panel of Figure 2 the dashed lines indicate the individual planetary signals and the solid line represents the combined signal. Next to each of

[2]`http://ssd.jpl.nasa.gov/?horizons`

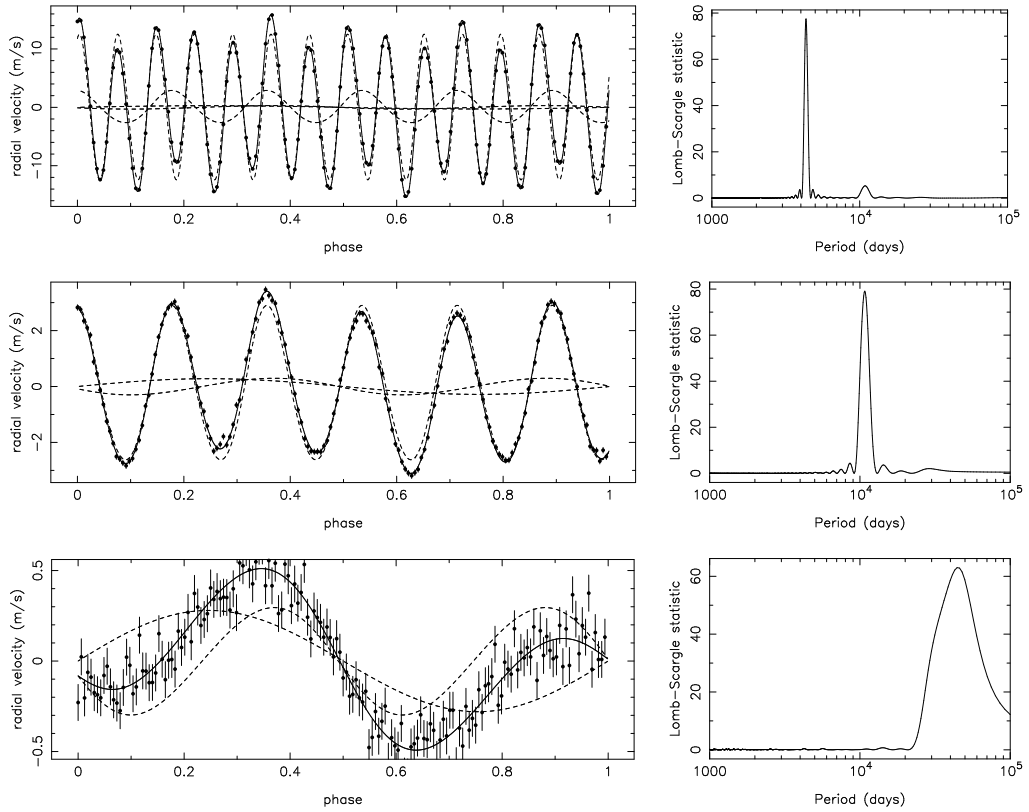

Figure 2: Combined radial velocity signature (solid lines) and individual planetary signatures (dashed lines) for the giant planets of our solar system, along with simulated radial velocity measurements with a cadence of ~ 1 year. The periodograms in the right panels show the Fourier analysis of the combined signals. The top panel includes Jupiter, Saturn, Uranus, and Neptune. The middle panel includes Saturn, Uranus, and Neptune. The bottom panel includes Uranus and Neptune. In each case, the orbital phase is normalized to the orbital period of Neptune.

Table 1: Radial velocity parameters of the giant planets.

Planet	P (days)	M_p (M_J)	e	K (m/s)
Jupiter	4332.820	1.000	0.049	12.47
Saturn	10755.698	0.299	0.056	2.76
Uranus	30687.153	0.046	0.044	0.30
Neptune	60190.029	0.054	0.011	0.28

the panels is a Lomb-Scargle (L-S) periodogram (Lomb, 1976; Scargle, 1982) from a Fourier analysis of the data. The Jupiter and Saturn signatures are clearly detected in their associated periodograms. The semi-amplitude of the Uranus and Neptune signatures are almost identical due to the lower mass of Uranus being compensated by its smaller orbital period. The Fourier disentanglement of the ice giant signatures is ambiguous with these data, although Keplerian orbital fitting will be more successful at extracting the independent parameters. Since the number of cycles is very limited, an approach which utilizes the Maximum Entropy Method (MEM) may be more helpful since this is relatively efficient in detecting frequency lines with few assumptions regarding the initial estimates of the fit parameters.

An important factor in the detection process is the eccentricity of the orbits. As shown in Table 1, the eccentricities for the solar system giant planets are all relatively low, less than 0.06. Many of the known exoplanets have eccentric orbits and the scattering of ice giants to larger semi-major axes, as described in Section 2, may contribute to this if other stabilizing influences are not present. Biases against the detection of non-zero eccentricities have been previously noted by Kane et al. (2007) and O'Toole et al. (2009) which may be resolved through the use of Keplerian periodograms and vigorously determined false-alarm thresholds (Cumming, 2004).

3.2. Detection vs Time

The ambiguous detection of Uranus and Neptune described in the previous section is partially due to the similar amplitudes of the radial velocity signals, but mostly due to the inadequate orbital periods monitored to produce a strong power in the Fourier spectrum. The dependence of a detection on the number of radial velocity measurements has been previously studied by Kane et al. (2007). Figure 3 shows how this ambiguity resolves when the system is monitored for two complete Neptunian orbital periods, still with a cadence of ~ 1 year. The resolution of the two distinct planetary signatures in the Fourier spectrum allows a Keplerian fit to easily recover the orbital parameters of the two planets.

3.3. Scaling to Low-mass Stars

A far more accessible parameter regime to probe in the near future is that surrounding the low mass stars. By combining the approximate location of the snow line (Ida & Lin, 2005) with Equation 1, we produce an expression

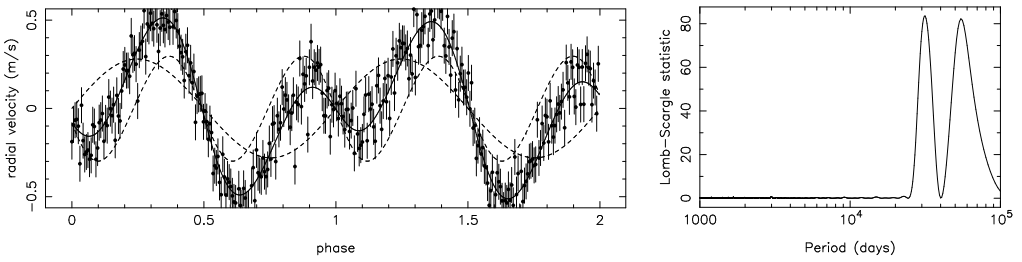

Figure 3: Combined radial velocity signature (solid lines) and individual planetary signatures (dashed lines) for Uranus and Neptune, along with simulated radial velocity measurements, after monitoring the host star for two Neptunian orbital periods. The periodogram in the right panel shows the Fourier analysis of the combined signal.

for the expected radial velocity semi-amplitude at the location of the snow line as a function of mass. This is given by

$$K = 18129 \times \frac{M_p \sin i}{M_\star^{5/6}(M_p + M_\star)^{2/3}} \frac{1}{\sqrt{1-e^2}} \tag{2}$$

where the mass of the planet and star are in units of solar masses for convenience. This expression may be considered an upper limit for the radial velocity signatures of possible ice giant analogues.

For example, if we placed a Neptune-mass planet at the snow line of a solar-mass star, the period of the orbit will be $\sim$ 1620 days and the semi-amplitude of the radial velocity signature will be $\sim$ 0.93 m/s. However, if the Neptune-mass planet were orbiting at the snow line of a late M dwarf (0.3 $M_\odot$) the period becomes $\sim$ 80 days and the semi-amplitude of the radial velocity signature rises to $\sim$ 5.7 m/s. This detection scenario is not only achievable, but has been significantly surpassed by current radial velocity surveys, indicating that we are now starting to build a picture of the frequency of Uranus/Neptune analogues around M dwarfs if not higher mass stars.

3.4. Linear Trends

According to the Exoplanet Data Explorer, 37 of the known radial velocity systems have measured linear trends in the residuals of the Keplerian orbital fitting. Of these, 9 are known to have a stellar companion which

may in some cases be the sources of the trend. The linear trends have amplitudes which lie in the range 0.0014–0.14 m/s/day. This is equivalent to 0.511–51.1 m/s/year which is already enough to exclude the detection of Uranus/Neptune analogues depending upon the mass of the host star and the timescale over which the trend has already been observed. Consider the case of HD 44219b (Naef et al., 2010), which has a minimum mass of $0.58 M_J$ and is in a 472 day orbit around a G2V star. The Keplerian solution for this planet includes a quadratric drift of 0.76390 m/s/year^2 which places this signature at the threshold of the expected semi-amplitude for a Neptune located at the snow line for a solar-type star, as described in Section 3.3. These kinds of trends will preferentially be caused by large mass objects since these produce larger signatures, but a greater time baseline is needed to resolve these potential ice giant detections.

4. Transit Signatures

The discovery of exoplanets using the transit technique has become increasingly dominant amongst the various detection methods. Examples of major contributors to the ground-based discovery of transiting exoplanets are the Hungarian Automated Telescope Network (HATNet) (Bakos et al., 2004) and SuperWASP (Pollacco et al., 2006). Ground-based surveys tend to be highly restricted in the period-space which they are able to sample, mostly due to the observational window function (von Braun et al., 2009). This is siginificantly improved by conducting such surveys from space, where the current major contributors are the Kepler mission (Borucki et al., 2010) and the CoRoT mission (Barge et al., 2008). The recent results released by the Kepler mission by Borucki et al. (2011) demonstrate that this mission is more than capable of detecting the signatures of Neptune-radii planets, though it will take further more time to detect these beyond the snow line for those stars in the Kepler Input Catalog (Brown et al., 2011).

The change in flux from the host star due to the transit of a planet is

$$\frac{\Delta F}{F} = \left(\frac{R_p}{R_\star}\right)^2 \tag{3}$$

where R_p and $R_\star$ are the radii of the planet and star respectively. The probability that a transit will be observable is given by

$$P_t = \frac{(R_p + R_\star)(1 + e\cos(\pi/2 - \omega))}{a(1 - e^2)} \tag{4}$$

where ω and a are the argument of periastron and semi-major axis of the orbit respectively (Kane & von Braun, 2008). Applying these to Neptune yield a transit depth of 0.13% and a transit probability of only 0.015%. Even though the photometric precision required is already achieved, it is difficult to imagine a survey that would monitor a star for 184 years with such small prospects for detecting a transit! If we consider a Neptune-radius planet at the snow line of a solar-type star, then the depth remains the same but the probability increases to 0.17%. As noted in Section 3.3, the orbital period in this case will be $\sim$ 1620 days. Thus the Kepler mission may well detect single transits from such ice giants during the mission duration. Scaling to low-mass stars, a Neptune-radius planet located at the snow line of a late M dwarf (0.3 $R_{\odot}$) results in a depth of 1.41% and a probability of 0.57%. These values place such planets well within the reach of Kepler and could even be detected by targetted transit searches of low-mass stars, such as the MEarth Project (Charbonneau et al., 2009).

5. Photometric Phase Signatures

As an exoplanet orbits the host star, the changing phase exhibits a distinct photometric signature. The photometric phase signatures of giant planets have been described in detail by Sudarsky et al. (2005) and Cahoy et al. (2010). However, the flux ratio of the planet to the host star is small compared to typical current photometric precisions and has presented a major hinderance to the realization of detecting such signatures. There is also the issue of stellar variability to contend with (see Section 3.1).

Investigating the giant planets of our solar system presents a significant challenge for even current space-based capabilities. Kane & Gelino (2010) and Kane & Gelino (2011) calculate the predicted amplitudes for giant planets in long-period orbits but only find detectable signatures during periastron passage for those in eccentric orbits. The flux ratio of the planet to the host star is defined as

$$\epsilon(\alpha, \lambda) \equiv \frac{f_p(\alpha, \lambda)}{f_\star(\lambda)} = A_g(\lambda) g(\alpha, \lambda) \frac{R_p^2}{r^2} \tag{5}$$

where α is the phase angle (defined to be zero at superior conjunction), λ is the wavelength, A_g is the geometric albedo, g is the phase function, and r is the star–planet separation. For the phase function, we adopt the "Hilton" function utilised by Kane & Gelino (2010) which is based upon

Table 2: Phase variation parameters of the giant planets.

Planet	P (days)	R_p (R_J)	e	A_g	$\epsilon_{\max}(10^{-9})$
Jupiter	4332.820	1.0000	0.049	0.52	4.845
Saturn	10755.698	0.8430	0.056	0.47	0.883
Uranus	30687.153	0.3575	0.044	0.51	0.037
Neptune	60190.029	0.3464	0.011	0.41	0.013

Pioneer observations of Venus and Jupiter. Table 2 contains the relevant orbital and physical parameters for this simulation, along with the predicted maximum flux ratios for each of the planets. The geometric albedos of the planets are well known and were also extracted from the JPL HORIZONS System.

Figure 4 shows the predicted phase signature for the solar system giant planets at optical wavelengths. The top panel includes all four planets. With each successive panel, the planetary signatures are removed in order of increasing semi-major axis until only the signature of Neptune remains. There are several key aspects to note here. Firstly, the amplitude of these signatures, shown in the figure and also in Table 2, are below what is currently accessible. For comparison, the ellipsoidal variations detected by Welsh et al. (2010) for the planet HAT-P-7b using Kepler data was of amplitude 3.7×10^{-5}. Secondly, this does not take into account ring structures such as the prominent ring system of Saturn (Dyudina et al., 2005), and so the phase signature is underestimated for some planets. Thirdly, these signatures are significantly lower than the solar variability, which was compared to the photometric variability found amongst Kepler stars by (Basri et al., 2010). The question of whether one could maintain precise photometric stability over long timescales is a related problem which is detector dependent. Fourthly, this does not include contamination from the terrestrial planets. As shown in Equation 5, the inverse relation of the star–planet separation will generally dominate over differences in planetary radii. Venus, for example, has an albedo of 0.65 which, combined with the much smaller semi-major axis, leads to a maximum flux ratio of 2.06×10^{-9} or 43% for that of Jupiter. Thus, the possible presence of much smaller terrestrial planets can not be ignored.

By using the same examples as those described in Section 3.3, we can test how this seemingly dire situation were to change if Neptune were to be found

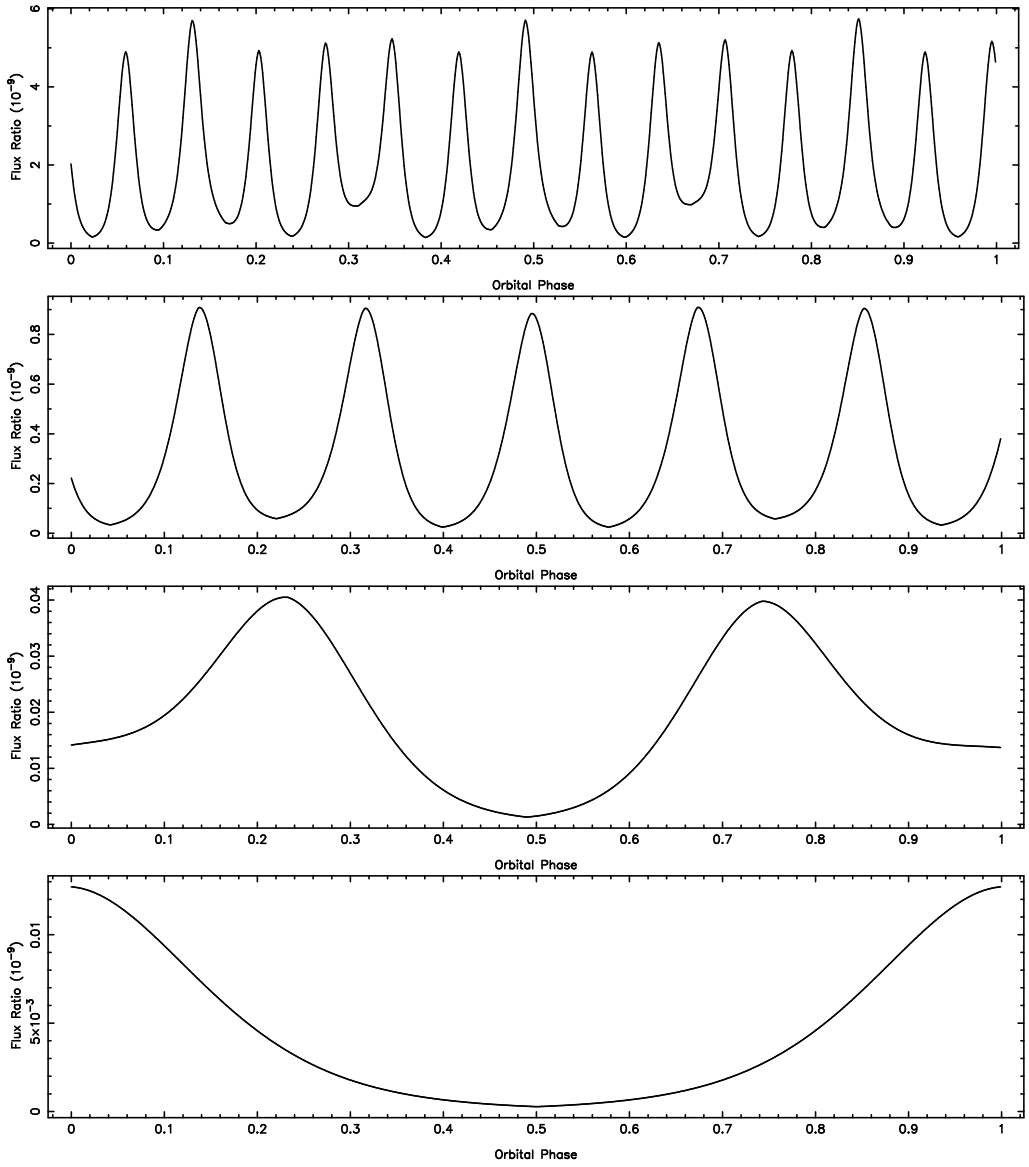

Figure 4: Combined phase signature for the giant planets of our solar system. The top panel includes Jupiter, Saturn, Uranus, and Neptune. Each successive panel removes the signature of a planet in order of their semi-major axis, ending with the phase signature of Neptune in the bottom panel. In each case, the orbital phase is normalized to the orbital period of Neptune.

in different situations. If we place Neptune at the snow line of a solar-type star ($P = 1620$ days), then the predicted maximum flux ratio increases to 1.57×10^{-9}, just slightly lower than that of Venus. If however, Neptune were to be located at the snow line of a late M dwarf ($P = 80$ days), then the predicted maximum flux ratio becomes 1.95×10^{-7}. This is two orders of magnitude below the flux ratio detected in HAT-P-7 by Welsh et al. (2010). However, such flux ratios are not beyond the reach of planned coronographic missions and thirty-meter class telescopes and may provide an opportunity to not only detect an ice giant but to characterize the atmosphere.

6. Astrometry and Imaging

The limits on using astrometry for detecting outer planets have been explored by Eisner & Kulkarni (2001), and further investigated by combining with radial velocity data by Eisner & Kulkarni (2002). Direct imaging of exoplanets has had recent success, such as the discovery of the planetary system orbiting the nearby star HR 8799 with semi-major axes as small as 14.5 AU (Marois et al., 2008, 2010). The techniques of astrometry and imaging are distinct from the previous two methods investigated as they (a) are more sensitive to long-period orbits and (b) depend upon the distance to the system. They are further distinctive in that they are more sensitive to face-on orbits rather than edge-on orbits for which the radial velocity, transit, and (often) phase variation techniques typically favour. An addition factor for the imaging technique is the dependence upon the age of the system since young planets (< 1 Gyr) will have self-luminous properties.

The amplitude of the astrometric signature is given by

$$\Delta\theta = \left(\frac{M_p}{M_\star}\right)\left(\frac{a}{d}\right) \tag{6}$$

According to the Exoplanet Data Explorer, the distribution of distances to the host stars for the known radial velocity planets peaks at ~ 35 pcs, due largely to the observational biases in the target selection. Neptune viewed from this distance has an angular separation from the Sun of 0.86 arcsec but a predicted astrometric signature of 44 μarcsec. However, a Neptune-mass planet located at the snow line of a late M dwarf has an angular separation of 0.007 arcsec and a predicted astrometric signature of 1.2 μarcsec. Thus, if such techniques are to be used for attempting the detection of ice giants, actual solar analogues are preferred targets over late-type stars. Current and

future coronographic experiments may play a role in probing the regime of ice giants as sensitvities and angular resolutions increase. Beichman et al. (2010), for example, tabulates the inner working angle of selected future ground-based imaging instruments which lie in the range 0.03–0.17 arcsec, compared to 0.035–0.850 arcsec for James Webb Space Telescope (JWST) instruments.

7. Conclusions

The formation and subsequent migration of ice giants appear to have played a major role in the overall formation and evolution of the outer solar system. Whether this is generally true of other solar-type systems and the frequency of such ice giants remains to be seen. The current sample of exoplanets is probing deeper into this regime in terms of mass but needs a longer time baseline to establish the period sensitivity to detect true Uranus/Neptune analogues. As existing radial velocity surveys continue to monitor known exoplanet hosting stars and simultaneously improve instrument precisions, the growing sample will slowly push further into the regime of the ice giants. The regime is also being explored by the Kepler and CoRoT missions using the transit technique from space where it is the mission duration and not the observational window function that constrains the detection of long-period planets. Detecting photometric phase variations poses significant technological challenges in the short-term and astrophysical challenges including intrinsic stellar variability and contamination from interior terrestrial planets.

The current situation favours exploring Neptune-mass planets beyond the snow line of late-type stars, where the required precision and timescales are significantly less, and will reveal the formation mechanisms in these environments. Results from the Kepler mission are allowing the study of transit timing variations which are sensitive enough to detect longer-period planets in those systems. In addition, continuing microlensing surveys have enough current sensitivity to provide a statistical census of ice giants through which we can determine the frequency of these objects, though not necessarily their orbital and physical characteristics. It has been demonstrated by Colón et al. (2010) that precision photometry of $< 0.05\%$ can be achieved with large telescopes through the use of narrow-band filters. Simulations of current and planned coronagraphs by Beichman et al. (2010) indicate that long-term stability may indeed be possible for exoplanet searches. Future

large ground-based telescopes, such as the European Extremely Large Telescope (E-ELT), the Thirty Meter Telescope (TMT), and the Giant Magellan Telescope (GMT), as well as space-based coronographic missions, may thus provide the needed precision for more direct detections via phase variation signatures and imaging.

Acknowledgements

The author would like to thank Kaspar von Braun, Jason Wright, Suvrath Mahadevan, and Chas Beichman for several useful discussions. I would also like to thank the referees, whose comments helped to improve the quality of this work. This research has made use of the Exoplanet Orbit Database and the Exoplanet Data Explorer at exoplanets.org.

References

Bakos, G., Noyes, R.W., Kovács, G., Stanek, K.Z., Sasselov, D.D., Domsa, I., 2004, Wide-Field Millimagnitude Photometry with the HAT: A Tool for Extrasolar Planet Detection, PASP, 116, 266-277

Barge, P., et al., 2008, Transiting exoplanets from the CoRoT space mission. I. CoRoT-Exo-1b: a low-density short-period planet around a G0V star, A&A, 482, L17-L20

Basri, G., et al., 2010, Photometric Variability in Kepler Target Stars: The Sun Among Stars-a First Look, ApJ, 713, L155-L159

Beichman, C.A., et al., 2010, Imaging Young Giant Planets From Ground and Space, PASP, 122, 162-200

Benvenuto, O.G., Fortier, A., Brunini, A., 2009, Forming Jupiter, Saturn, Uranus and Neptune in few million years by core accretion, Icarus, 204, 752-755

Boisse, I., Bouchy, F., Hebrard, G., Bonfils, X., Santos, N.C., Vauclair, S., 2011, Disentangling between stellar activity and planetary signals, A&A, 528, 4-14

Borucki, W.J., et al., 2010, Kepler Planet-Detection Mission: Introduction and First Results, Science, 327, 977-980

Borucki, W.J., et al., 2011, Characteristics of planetary candidates observed by Kepler, II: Analysis of the first four months of data, ApJ, submitted (arXiv:1102.0541)

Boss, A.P., 2006, Rapid Formation of Gas Giant Planets around M Dwarf Stars, ApJ, 643, 501-508

Boss, A.P., 2010, Giant Planet Formation by Disk Instability in Low Mass Disks?, ApJ, 725, L145-L149

Brown, T.M., Latham, D.W., Everett, M.E., Esquerdo, G.A., 2011, Kepler Input Catalog: Photometric Calibration and Stellar Classification, AJ, submitted (arXiv:1102.0342)

Cahoy, K.L., Marley, M.S., Fortney, J.J., 2010, Exoplanet Albedo Spectra and Colors as a Function of Planet Phase, Separation, and Metallicity, ApJ, 724, 189-214

Charbonneau, D., et al., 2009, A super-Earth transiting a nearby low-mass star, Nature, 462, 891-894

Colón, K.D., Ford, E.B., Lee, B., Mahadevan, S., Blake, C.H., 2010, Characterizing transiting extrasolar planets with narrow-band photometry and GTC/OSIRIS, MNRAS, 408, 1494-1501

Cumming, A., 2004, Detectability of extrasolar planets in radial velocity surveys, MNRAS, 354, 1165-1176

Dodson-Robinson, S.E., Bodenheimer, P., 2010, The formation of Uranus and Neptune in solid-rich feeding zones: Connecting chemistry and dynamics, Icarus, 207, 491-498

Dyudina, U.A., Sackett, P.D., Bayliss, D.D.R., Seager, S., Porco, C.C., Throop, H.B., Dones, L., 2005, Phase Light Curves for Extrasolar Jupiters and Saturns, ApJ, 618, 973-986

Eisler, J.A., Kulkarni, S.R., 2001, Sensitivity of the Astrometric Technique in Detecting Outer Planets, ApJ, 561, 1107-1115

Eisler, J.A., Kulkarni, S.R., 2002, Detecting Outer Planets in Edge-on Orbits: Combining Radial Velocity and Astrometric Techniques, ApJ, 574, 426-429

Ford, E.B., Chiang, E.I., 2007, The Formation of Ice Giants in a Packed Oligarchy: Instability and Aftermath, ApJ, 661, 602-615

Fortney, J.J., Ikoma, M., Nettelmann, N., Guillot, T., Marley, M.S., 2011, Self-consistent Model Atmospheres and the Cooling of the Solar System's Giant Planets, ApJ, 729, 32-45

Gould, A., et al., 2010, Frequency of Solar-like Systems and of Ice and Gas Giants Beyond the Snow Line from High-magnification Microlensing Events in 2005-2008, ApJ, 720, 1073-1089

Ida, S., Lin, D.N.C., 2005, Toward a Deterministic Model of Planetary Formation. III. Mass Distribution of Short-Period Planets around Stars of Various Masses, ApJ, 626, 1045-1060

Kane, S.R., Schneider, D.P., Ge, J., 2007, Simulations for multi-object spectrograph planet surveys, MNRAS, 377, 1610-1622

Kane, S.R., von Braun, K., 2008, Constraining Orbital Parameters through Planetary Transit Monitoring, ApJ, 689, 492-498

Kane, S.R., Gelino, D.M., 2010, Photometric Phase Variations of Long-period Eccentric Planets, ApJ, 724, 818-826

Kane, S.R., Gelino, D.M., 2011, On the Inclination Dependence of Exoplanet Phase Signatures, ApJ, 729, 74-79

Kennedy, G.M., Kenyon, S.J., Bromley, B.C., 2006, Planet Formation around Low-Mass Stars: The Moving Snow Line and Super-Earths, ApJ, 650, L139-L142

Kennedy, G.M., Kenyon, S.J., 2008, Planet Formation around Stars of Various Masses: The Snow Line and the Frequency of Giant Planets, ApJ, 673, 502-512

Lagrange, A.-M., Desort, M., Meunier, N., 2010, Using the Sun to estimate Earth-like planets detection capabilities . I. Impact of cold spots, A&A, 512, 38-52

Levison, H.F., Morbidelli, A., VanLaerhoven, C., Gomes, R., Tsiganis, K., 2008, Origin of the structure of the Kuiper belt during a dynamical instability in the orbits of Uranus and Neptune, Icarus, 196, 258-273

Li, C.-H., et al., 2008, A laser frequency comb that enables radial velocity measurements with a precision of 1cms^{-1}, Nature, 452, 610-612

Lomb, N.R., 1976, Least-squares frequency analysis of unequally spaced data, Ap&SS, 39, 447-462

Makarov, V.V., Beichman, C.A., Catanzarite, J.H., Fischer, D.A., Lebreton, J., Malbet, F., Shao, M., 2009, Starspot Jitter in Photometry, Astrometry, and Radial Velocity Measurements, ApJ, 707, L73-L76

Marois, C., Macintosh, B., Barman, T., Zuckerman, B., Song, I., Patience, J., Lafreniére, D., Doyon, R., 2008, Direct Imaging of Multiple Planets Orbiting the Star HR 8799, Science, 322, 1348-1352

Marois, C., Zuckerman, B., Konopacky, Q.M., Macintosh, B., Barman, T., 2010, Images of a fourth planet orbiting HR 8799, Nature, 468, 1080-1083

Matsuo, T., Shibai, H., Ootsubo, T., Tamura, M., 2007, Planetary Formation Scenarios Revisited: Core-Accretion versus Disk Instability, ApJ, 662, 1282-1292

Mayor, M., et al., 2009, The HARPS search for southern extra-solar planets. XVIII. An Earth-mass planet in the GJ 581 planetary system, A&A, 507, 487-494

Meunier, N., Lagrange, A.-M., Desort, M., 2010, Reconstructing the solar integrated radial velocity using MDI/SOHO, A&A, 519, 66-73

Murphy, M.T., et al., 2007, High-precision wavelength calibration of astronomical spectrographs with laser frequency combs, MNRAS, 380, 839-847

Naef, D., et al., 2010, The HARPS search for southern extrasolar planets. XXIII. 8 planetary companions to low-activity solar-type stars, A&A, 523, 15-22

O'Toole, S.J., Tinney, C.G., Jones, H.R.A., Butler, R.P., Marcy, G.W., Carter, B., Bailey, J., 2009, Selection functions in doppler planet searches, MNRAS, 392, 641-654

Pepe, F.A., Lovis, C., 2008, From HARPS to CODEX: exploring the limits of Doppler measurements, Physica Scripta Volume T, 130, 014007-014016

Pollacco, D.L., et al., 2006, The WASP Project and the SuperWASP Cameras, PASP, 118, 1407-1418

Rivera, E.J., Laughlin, G., Butler, R.P., Vogt, S.S., Haghighipour, N., Meschiari, S., 2010, The Lick-Carnegie Exoplanet Survey: a Uranus-Mass Fourth Planet for GJ 876 in an Extrasolar Laplace Configuration, ApJ, 719, 890-899

Scargle, J.D., 1982, Studies in astronomical time series analysis. II - Statistical aspects of spectral analysis of unevenly spaced data, ApJ, 263, 835-853

Simpson, E.K., Baliunas, S.L., Henry, G.W., Watson, C.A., 2010, Rotation periods of exoplanet host stars, MNRAS, 408, 1666-1679

Sudarsky, D., Burrows, A., Hubeny, I., Li, A., 2005, Phase Functions and Light Curves of Wide-Separation Extrasolar Giant Planets, ApJ, 627, 520-533

Steinmetz, T., et al., 2008, Laser Frequency Combs for Astronomical Observations, Science, 321, 1335-1337

Strassmeier, K.G., 2009, Starspots, A&ARv, 17, 251-308

Thommes, E.W., Duncan, M.J., Levison, H.F., 1999, The formation of Uranus and Neptune in the Jupiter-Saturn region of the Solar System, Nature, 402, 635-638

Thommes, E.W., Duncan, M.J., Levison, H.F., 2002, The Formation of Uranus and Neptune among Jupiter and Saturn, ApJ, 123, 2862-2883

Udem, Th., Holzwarth, R., Hänsch, T.W., 2002, Optical frequency metrology, Nature, 416, 233-237

von Braun, K., Kane, S.R., Ciardi, D.R., 2009, Observational Window Functions in Planet Transit Surveys, ApJ, 702, 779-790

Welsh, W.F., Orosz, J.A., Seager, S., Fortney, J.J., Jenkins, J., Rowe, J.F., Koch, D., Borucki, W.J., 2010, The Discovery of Ellipsoidal Variations in the Kepler Light Curve of HAT-P-7, ApJ, 713, L145-L149

Wright, J.T., 2005, Radial Velocity Jitter in Stars from the California and Carnegie Planet Search at Keck Observatory, PASP, 117, 657-664

Wright, J.T., Marcy, G.W., Butler, R.P., Vogt, S.S., Henry, G.W., Isaacson, H., Howard, A.W., 2008, The Jupiter Twin HD 154345b, ApJ, 683, L63-L66